ROUGHNESS AND RADAR POLARIMETRY OF LUNAR POLAR CRATERS: TESTING FOR ICE DEPOSITS. B. J. Thomson[1], P. D. Spudis[2], D. B. J. Bussey[1], L. Carter[3], R. L. Kirk[4], C. Neish[1], G. Patterson[1], R. K. Raney[1], H. Winters[1], and the Mini-RF Team. [1]JHU Applied Physics Lab, Laurel MD 20723 (bradley.thomson@jhuapl.edu); [2]Lunar and Planetary Inst., Houston, TX; [3]Smithsonian Inst., Washington DC; [4]USGS, Flagstaff, AZ.

Introduction: Planetary bodies with spin axes near perpendicular to the ecliptic have been recognized to potentially harbor volatile deposits in permanently shadowed cold traps in their polar regions [1]. Radar measurements can be used to discriminate between ice and silicate material in these cold traps that, by definition, receive no direct solar illumination. Thick deposits of ice, for example, have circular polarization ratios (CPR or μ_c) that exceed unity [2]. Earth-based radar observations have detected signatures consistent with water ice in the polar regions of Mercury [3]. Both terrestrial and orbital radars have detected near-polar surfaces on the Moon with enhanced CPR, though interpretations differ as to the cause [e.g., 4, 5]. Fresh, rough craters, for example, also exhibit high values of CPR.

Initial results from the Mini-SAR instrument on the Chandrayaan-1 spacecraft reveal a population of polar craters with high CPR values consistent with ice [6, 7]. Here, we report on the slope and roughness characteristics of some of these craters to aid discrimination between those that are potentially ice-bearing from those that are rough but ice-free.

Data Description: The Mini-SAR instrument utilizes a unique hybrid dual-polarization architecture to transmit a circularly polarized incident radar beam and coherently receive the linear horizontal and vertical components [8, 9]. Operating in the S-band (2380 MHz, 12.6 cm wavelength) with a nominal incidence angle of 33.5°, the instrument returned data in SAR mode (synthetic aperture radar) at a ground sample distance of 75 m/pixel. Radar measurements of both polar regions of the Moon down to about 80° N and S latitude were acquired in the first imaging season from February to April, 2009. Data from a second partial imaging season were obtained in late August, and the mission was declared terminated on 30 August 2009 due to a loss of communication with Chandrayaan-1.

CPR background. A useful potential identifying characteristic of water ice is the circular polarization ratio of the returned radar signal, which is defined as the ratio of the same sense circular polarization (SC) to the opposite sense of polarization (OC). Ice deposits, normally a relative lossless medium to radar, exhibit high CPR values that have been attributed to volumetric scattering from internal inhomogeneities [10, 11]. Additionally, high CPR return is also observed from non-ice surfaces that are rough at the wavelength of the incident radar. CPR values were calculated from Mini-SAR measurements using the four Stokes parameters of the backscattered field.

Results: Results for a portion of the lunar north polar region are given in Figure 1. Areas with enhanced CPR values (indicated by orange and red tones) are limited to small craters both within and between larger impact structures.

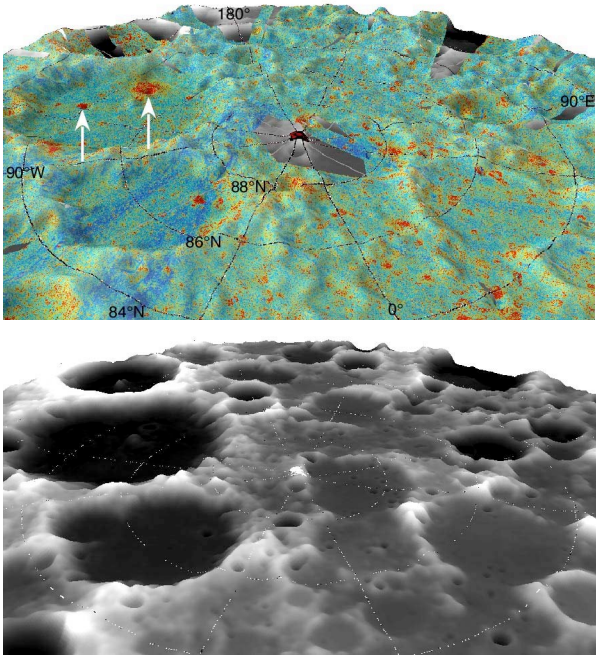

Figure 1. (Top) Perspective view of a colorized map of CPR from Mini-SAR measurements of the lunar north pole draped over a shaded relief map (polar stereographic projection). Orange and red colors indicate regions of enhanced CPR. White arrows indicate positions of craters given in Fig. 2. **(Bottom)** Same view as above with only topographic data [12]. Vertical exaggeration is 4x.

Closer inspection of these impact structures with high CPR values reveal two distinct populations, as noted by [6, 7]. The first population consist of fresh, presumably relatively more recent impact craters (Figure 2A-B, crater profile *a-a'*). Craters with radar bright ejecta and interiors have been observed elsewhere on the Moon [e.g., 13], and their radar signature has been attributed to an excess of surface or near-surface rocks relative to the surrounding terrain. Profiles though this crater (labeled *a-a'*) are given in Fig. 2E-F showing surface slopes (~500 m baseline) derived from Selene topographic data [12] and CPR val-

ues derived from Mini-SAR data. In Fig. 2E, interior surface slopes attain a maximum of ~31° while exterior slopes peak at about 6°. Although corresponding CPR values are elevated throughout the crater interior (typical values 0.8-1.4), exterior values are also high (0.6-0.8).

A representative of a second, distinct population of craters is given in crater profile *b-b'* (Fig. 2A-B). This crater possesses an enhanced CPR value inside the central cavity (0.8 to 1.6), but the enhancement fades to background immediately outside the crater rim (Fig. 2D). Additionally, this crater exhibits shallower wall slopes (maximum 26°) and lower slopes in the proximal ejecta facies than the fresh crater example. The crater rim height is also lower than the fresh crater example, but the difference in crater size negates a direct comparison without scaling. These morphologic characteristics are consistent with the second crater being a relatively older, more degraded crater. Continued micrometeoroid bombardment and gardening tends to subdue slopes and break down rocks over time, leading to shallower crater wall slopes, enlargement of the crater diameter, and a more subdued overall appearance.

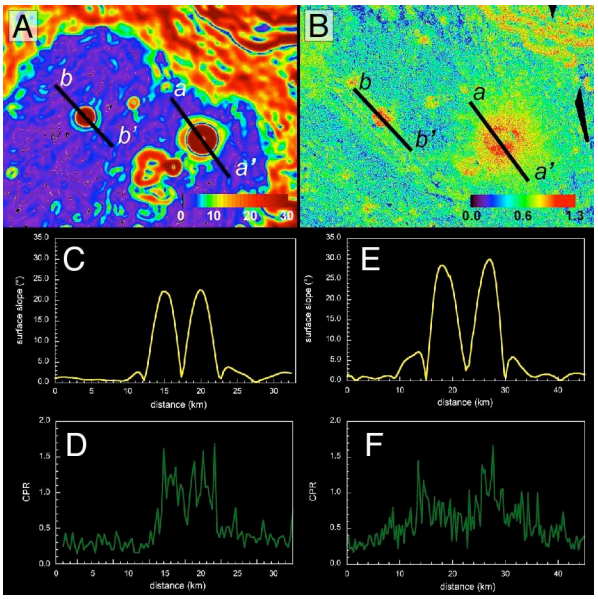

Figure 2. Craters on floor of Rozhdestvensky (near 85°N, 175°W). **(A)** Surface slopes measured on a 500 m baseline from Selene topographic data. **(B)** CPR mosaic from Mini-SAR data. **(C-D)** Profiles through crater *b-b'* of slope (top, yellow curve) and CPR (bottom, green curve). **(E-F)** Profiles through fresh crater *a-a'* of slope and CPR, respectively.

One caveat with these straight-line profiles is that no correction has been made for distortion introduced by the side-looking radar viewing geometry. For example, the floors of craters appear to be displaced away from the observer prior to applying a terrain correction. Since the initial SAR processing is done assuming a uniform lunar sphere, more advanced reprocessing of the data using high-resolution topographic data and a network of established tie points will be necessary to fully correct for this layover effect [14].

A 2D scatterplot of CPR versus surface slope is given in Fig. 3. Although the aforementioned terrain distortion introduces some uncertainty, no clear correction between these two parameters is evident in the scene. The moderately high CPR annulus surrounding the fresh crater occupies a somewhat unique portion of the plot (outlined in green in Fig. 2B and 3) of low slopes (2-8°) but high CPR values (>0.8).

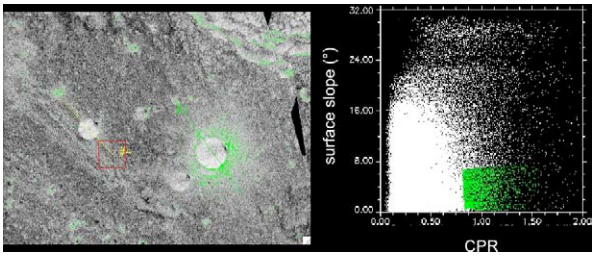

Figure 3. (Left) Grayscale version of Fig. 2B. **(Right)** 2D scatterplot of surface slopes (on y-axis, from Fig 2A) versus CPR values (on x-axis, from Fig. 2B). Region of plot highlighted in green is also colored green in grayscale image on left and largely corresponds to crater ejecta.

Discussion: The first population of craters with enhanced CPR values is fully consistent with fresh craters. Our current working hypothesis is that the elevated CPR in the interiors of the second crater population is due to the presence of ice. If members of the second population were just degraded versions of the former category, one would expect at least some reduction of the CPR values in the crater interior due to degradation of the expected higher rock abundance (the presumed cause of high CPR in the first population). Instead, the opposite is trend observed – craters in the second population tend to have higher interior CPR values than craters in the first population. In summary, our preliminary analysis of these examples suggests that slope/roughness effects alone do not fully account for the enhanced CPR signatures of certain crater interiors in permanently shadowed regions of the north polar region of the Moon.

References: [1] Urey H. C. (1952) *The Planets: Their Origin and Development*, 245 pp. [2] Ostro S.J. *et al.* (1992) *JGR*, *97*, 18277-18244. [3] Slade M.A. *et al.* (1992) *Science*, *258*, 635-640. [4] Nozette S. *et al.* (1996) *Science*, *274*, 1495-1498. [5] Campbell D.B. *et al.* (2006) *Nature*, *443*, 835-837. [6] Spudis P.D. *et al.* (this volume) *LPS XLI*. [7] Spudis P.D. *et al.* (in prep.) *GRL*. [8] Raney R.K. (2007) *IEEE Trans. Geosci. Rem. Sen.*, *45*, 3397-3404. [9] Spudis P. *et al.* (2009) *Current Science (India)*, *96*, 533-539. [10] Hapke B. (1990) *Icarus*, *88*, 407-417. [11] Hagfors T. *et al.* (1997) *Icarus*, *130*, 313-322. [12] Araki H. *et al.* (2009) *Science*, *323*, 897-900. [13] Thompson T.W. *et al.* (1981) *Icarus*, *46*, 201-225. [14] Kirk R. *et al.* (volume) *LPS XLI*.